Structure
Resource

Dramatic Improvement of Crystals of Large RNAs by Cation Replacement and Dehydration

Jinwei Zhang[1] and Adrian R. Ferré-D'Amaré[1,*]
[1]National Heart, Lung and Blood Institute, 50 South Drive, MSC 8012, Bethesda, MD 20892-8012, USA
*Correspondence: adrian.ferre@nih.gov
http://dx.doi.org/10.1016/j.str.2014.07.011

SUMMARY

Compared to globular proteins, RNAs with complex 3D folds are characterized by poorly differentiated molecular surfaces dominated by backbone phosphates, sparse tertiary contacts stabilizing global architecture, and conformational flexibility. The resulting generally poor order of crystals of large RNAs and their complexes frequently hampers crystallographic structure determination. We describe and rationalize a postcrystallization treatment strategy that exploits the importance of solvation and counterions for RNA folding. Replacement of Li^+ and Mg^{2+} needed for growth of crystals of a tRNA-riboswitch-protein complex with Sr^{2+}, coupled with dehydration, dramatically improved the resolution limit (8.5–3.2 Å) and data quality, enabling structure determination. The soft Sr^{2+} ion forms numerous stabilizing intermolecular contacts. Comparison of pre- and posttreatment structures reveals how RNA assemblies redistribute as quasi-rigid bodies to yield improved crystal packing. Cation exchange complements previously reported postcrystallization dehydration of protein crystals and represents a potentially general strategy for improving crystals of large RNAs.

INTRODUCTION

Novel noncoding RNAs are being discovered rapidly through the application of next-generation sequencing and genomic technologies. Many of these RNAs have been implicated in important cellular processes, but elucidation of their molecular mechanisms of action is often hampered by the paucity of structural information (Wan et al., 2011). X-ray crystallography is the method of choice for the structural determination of large RNAs and RNA-protein complexes. However, it is rare for crystals of RNAs with complex 3D structures to diffract X-rays to resolutions useful for biochemical insight, i.e., ~3.5 Å or better (Ferré-D'Amaré, 2010; Ferré-D'Amaré et al., 1998). Although several postcrystallization treatments that improve the quality of protein crystals have been described (Heras and Martin, 2005), comparable methods have not been well documented in the challenging arena of RNA crystallography.

Recently, we reported the crystal structure of a ternary complex formed between the complete Stem I domain of a T-box riboswitch, its cognate tRNA, and the RNA-binding protein YbxF (Zhang and Ferré-D'Amaré, 2013). Although structures of some of the isolated components of this complex had been previously reported (Baird et al., 2012; Grigg et al., 2013), the cocrystal structure allowed visualization of a gene-regulatory tRNA-mRNA complex formed outside the context of a translating ribosome for the first time (Chetnani and Mondragón, 2013; Zhang and Ferré-D'Amaré, 2013). Successful structure determination was made possible by a novel postcrystallization treatment that combines cation replacement and dehydration, which improved the diffraction limit of the crystals from ~8 to ~3 Å resolution. We have now systematically examined the effect of individual treatments alone and in combination. Our analysis reveals distinct roles of Sr^{2+} in stabilizing RNA structure and bridging RNA-RNA packing interactions, in particular, through specific binding to RNA terminal *cis*-diols. To illuminate the underlying physical basis for the dramatic improvement in crystal order, we determined and compared a series of structures of crystals subjected to a variety of postcrystallization treatments, including the untreated crystals (that diffract to only ~8.5 Å resolution). Structural comparison allows us to track how the RNA molecules reorient in the crystals and how such shifts generate improved crystal-packing contacts that ultimately lead to the improvement in crystalline order.

RESULTS

Dehydration and Cation Replacement Synergistically Improve Crystals

Square, plate-shaped cocrystals containing the ternary complex of *Oceanobacillus iheyensis glyQ* T-box Stem I RNA, a circularly permuted *Bacillus subtilis* $tRNA^{Gly}$, and *B. subtilis* YbxF protein grew optimally in the presence of 50 mM Bis(2-hydroxyethyl)-amino-tris(hydroxymethyl)-methane (Bis-Tris) (pH 6.5), 0.3 M Li_2SO_4, 20 mM $MgCl_2$ and 20% (w/v) polyethylene glycol 3350 (PEG 3350). When examined using rotation photography using synchrotron radiation, these crystals diffracted X-rays only to 8 Å resolution. Moreover, the Bragg spots were irregular and streaky, hampering data collection (Figure 1A). In an effort to improve the quality of these crystals, we tested a wide variety of postcrystallization treatment strategies. Ultimately, cocrystals grown in those conditions were incubated in a solution from which the Li_2SO_4 was omitted, 20 mM $MgCl_2$ was replaced with 40 mM $SrCl_2$, and the concentration of PEG 3350 was raised to 40%–48% (w/v). The combined dehydration and cation exchange substantially improved the diffraction spot profiles and data quality (Figure 1), dramatically extended the resolution of useful data (Table 1), enabled the identification of the two

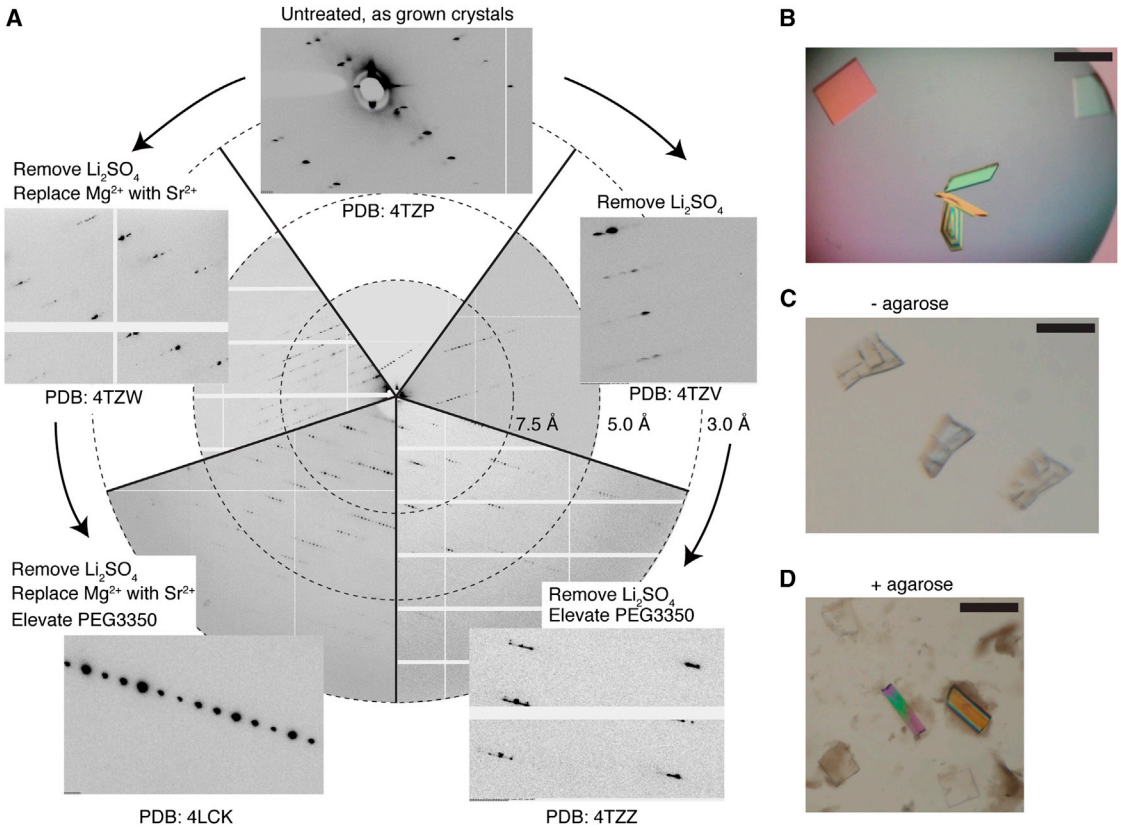

Figure 1. Effect of Cation Replacement and Dehydration on Diffraction Quality of Crystals of a T-Box Riboswitch-tRNA-YbxF Ternary Complex

(A) Portions of rotation photographs demonstrating the diffraction properties of untreated (as-grown) crystals (top, PDB code 4TZP), partially treated crystals (left, right, and lower right, PDB codes 4TZV, 4TZW, and 4TZZ), and crystals that were subjected to full cation replacement and dehydration (lower left, PDB code 4LCK). Magnified insets demonstrate the improvement in spot profile and order-to-order separation. Arrows indicate the progressive additions of treatments. Postcrystallization treatment and crystal properties are summarized in Table 1.

(B) Initially grown plate-like crystals of the T-box riboswitch-tRNA-YbxF ternary complex.

(C) Crystals in (B), grown in 20% PEG 3350 crack and disintegrate upon exposure to 40%–50% PEG 3350 in the dehydration solution.

(D) Same crystals grown in the presence of ~0.2% low-melting agarose exhibit drastically reduced cracking when exposed to the same dehydration solution. The crystals in this micrograph have been dissected from the gellified agarose network.

Scale bars in (B)–(D) represent 200 μm.

selenium atoms present in the 66 kDa complex for experimental phasing by single-wavelength anomalous dispersion (SAD), and allowed the refinement of the structure at 3.2 Å resolution. Presumably in response to the large, sudden osmolarity change due to increased PEG concentration, most crystals developed cracks and disintegrated quickly. To reinforce them, we grew crystals under the same conditions but in the presence of ~0.2% (w/v) low-melting-point agarose. Although infrequently used, in-gel crystallization using agarose, silica, or other gel matrices has been reported to produce crystals comparable in quality to those grown under microgravity (Chayen, 2004), due to the reduction of nucleation events, suppression of convection, and improved mechanical properties (Lorber et al., 2009). Previously, the inclusion of 0.01% agarose aided the crystallization of a *B. stearothermophilus* RNase P variant (Kazantsev et al., 2009). The use of agarose not only increased the thickness of our plate-like T-box ternary-complex crystals but greatly reduced the frequency and extent of crystal cracking during the treatment, presumably due to the presence of agarose fibers randomly deposited inside crystal solvent channels (Lorber et al., 2009).

To identify the factors underlying the success of our postcrystallization treatment strategy, we analyzed separately the effect of the removal of Li_2SO_4, exchange of Mg^{2+} with Sr^{2+}, or increase in PEG concentration, and found that one of these individual treatments alone only modestly improved the diffraction limit (from 8.5 to 5.0 Å), implying synergy among them (Figure 1A and Table 1). Removal of Li_2SO_4 (whose presence was required for the growth of robust, single crystals) alone did partially improve the diffraction limit but not the Bragg reflection profiles. Removal of Li_2SO_4, combined with an increase in PEG and Mg^{2+} concentration (e.g., to 40% and 100 mM, respectively) could, in some cases, increase the resolution of the crystals to ~3.2 Å. However, the Bragg-spot profiles of crystals treated in this manner remained poor. Despite exhaustive screening of several hundred crystals and a variety of treatment schemes, the only

Table 1. Select Properties of Crystals Treated with Varying Degrees of Ion Replacement and Dehydration

PDB Code	Li_2SO_4 (mM)	$MgCl_2$ (mM)	$SrCl_2$ (mM)	PEG 3350 (% w/v)	Resolution (Å)	Space Group	Unit Cell Dimensions (Å)	V_M (Å^3/Da)[a]	V_S (%)[b]
4TZP	300	20	0	20	8.5	$C222_1$	108.7, 108.8, 291.8[c]	3.27	62.4
4TZV	0	20	0	20	5.0	$P4_32_12$	75.7, 75.7, 270.2[c]	2.93	58.1
4TZW	0	0	50	20	4.7	$P4_32_12$	75.3, 75.3, 268.9[c]	2.89	57.4
4TZZ	0	100	0	48	3.6	$P2_1$	70.6, 260.7, 70.7[d]	2.46	50.0
4LCK	0	0	40	40	3.2	$C222_1$	100.3, 108.4, 266.8[c]	2.75	55.2

[a] V_M Matthews coefficient (Matthews, 1968).
[b] V_s calculated solvent content.
[c] $\alpha = \beta = \gamma = 90°$.
[d] $\alpha = \gamma = 90°$; $\beta = 92.8°$.

data sets that produced sufficiently resolved Bragg reflection profiles (and correspondingly high-quality data) for SAD phasing came from crystals that had undergone exchange of Mg^{2+} with Sr^{2+} in addition to removal of Li_2SO_4 and increase in PEG concentration. Interestingly, the presence of Ba^{2+}, a commonly used phasing heavy atom, strongly degrades the diffracting quality of these crystals, presumably due to its larger ionic radius than Sr^{2+}. These results suggest that, among the cations tested, Sr^{2+} uniquely improves the long-range order of T-box ternary-complex crystals.

Rigid-Body RNA Rearrangements Yield Improved Crystal Packing

To visualize the response of the RNA complexes in the crystal to cation substitution and dehydration, we determined the structures of untreated crystals and of crystals subjected to various postcrystallization treatments (Tables 1 and 2; Experimental Procedures). Superposition of structures of the ternary complexes in the differently treated crystals demonstrates that the T-box-tRNA-YbxF ternary complexes rearranged essentially as rigid bodies (Figure 2; root-mean-square deviation [rmsd] of 0.9–1.4 Å for all C1′ atom pairs). The improvement in crystal packing and the concurrent reduction in solvent content of the T-box RNA crystals resulting from postcrystallization treatments (Table 1) arise from rotations and translations of neighboring complexes (Figure 2). These bring three neighboring ternary complexes related by crystallographic symmetry into closer proximity, enabling the formation of intimate stacking interactions between two patches on the rear face of the interdigitated T-loops (opposite the face interacting with the tRNA elbow; Zhang and Ferré-D'Amaré, 2013) of one complex with the apical adenine of the GAAA tetraloop capping the tRNA acceptor stem of a second complex and also with the terminal base pair of Stem I of a third (compare Figures 3A and 3B). Notably, these movements also enable the formation of an energetically favorable class-I A-minor interaction (Nissen et al., 2001) between the last adenine of the GAAA tetraloop (engineered into the tRNA; Zhang and Ferré-D'Amaré, 2014b) of one complex and the minor groove of the Stem I proximal region of a symmetry-related complex (Figure 3D). This crystal contact is present only in the optimally treated crystals and is probably partly responsible for the dramatic improvement in diffraction limit and Bragg reflection profiles (Figure 1) brought about by full cation replacement and dehydration.

Pervasive Sr^{2+} Binding Uniquely Improves RNA Crystal Quality

For large RNAs to fold into their functional, compact conformations (and, analogously, to pack into crystals), counterions are required to offset the repulsion of the negatively charged backbone phosphates (Draper, 2004). Among divalents, alkaline earth metal ions (Mg^{2+}, Ca^{2+}, Sr^{2+}, Ba^{2+}) stand out as enablers of folding or catalysis for most riboswitches and ribozymes (Ferré-D'Amaré and Scott, 2010; Ferré-D'Amaré and Winkler, 2011; Zhang et al., 2010). The ionic radius, coordination number and geometry, hardness, and hydration enthalpy vary substantially among these ions. Our findings from the T-box cocrystals emphasize the importance of screening for the most suitable counterion to stabilize RNA, not only during crystallization but in postcrystallization treatments as well. Sr^{2+} is considerably softer than Mg^{2+} and Ca^{2+}, is smaller than Ba^{2+}, and has a coordination number up to 10–11 due to its larger radius (Hofer et al., 2006). Importantly, unlike the highly constrained octahedral (hexacoordinate) and pentagonal bipyramidal (octacoordinate) coordination geometries of Mg^{2+} and Ca^{2+}, Sr^{2+} exhibits considerable flexibility and ligand mobility and thus tolerates appreciable distortions of its trigonal prism coordination geometry (Hofer et al., 2006); these properties may make it a particularly advantageous cation for RNA crystal stabilization.

Comparison of T-box-tRNA-YbxF cocrystal structures containing Sr^{2+} ions with Mg^{2+}-only counterparts reveals that Sr^{2+}-binding sites on these RNAs are abundant (34 Sr^{2+} ions per 177 nucleotides) and reproducible among different crystals. Importantly, the structures of the ternary complex in the presence and absence of Sr^{2+} superimpose closely (rmsd < 1.0 Å), suggesting that pervasive Sr^{2+} binding does not distort the local or global structures of either the T-box RNA or tRNA, or their interaction. Interestingly, strong Sr^{2+} electron density is present adjacent to the 3′-terminal *cis*-diol of Stem I (Figure 4A; the 3′ terminus of the circularly permuted tRNA is intrahelical and does not bind Sr^{2+}). This Sr^{2+} bridges two T-box RNA molecules related by crystallographic symmetry through inner-sphere coordination and may thus contribute to improved crystal order. A similarly positioned Sr^{2+} ion bridges two symmetry-related 3′ *cis*-diols in crystals of a heptanucleotide derived from $tRNA^{Ala}$ acceptor stem (Figure 4B). The addition of Sr^{2+} improved the diffraction limit of those crystals (Mueller et al., 1999) from 1.7 to 1.16 Å. The specific binding of Sr^{2+} to RNA 3′ *cis*-diols is further exemplified by the crystal structure of a quadruplex-forming RNA (Figure 4C; Pan et al., 2006). In addition to interactions at

Table 2. Crystallographic Statistics for T-Box Ternary-Complex Structures

	PDB Accession Code				
	4TZP	4TZV	4TZW	4TZZ	4LCK
Data Collection					
Space group	$C222_1$	$P4_32_12$	$P4_32_12$	$P2_1$	$C222_1$
Cell length: *a*, *b*, *c* (Å)	108.7, 108.8, 291.8	75.7, 75.7, 270.2	75.3, 75.3, 268.9	70.6, 260.7, 70.7	100.3, 108.4, 266.8
Cell angles: α, β, γ (°)	90, 90, 90	90, 90, 90	90, 90, 90	90, 92.8, 90	90, 90, 90
Resolution (Å)[a]	48.63-8.50 (8.81-8.50)	46.03 - 5.03 (5.20 - 5.03)	45.79-4.67 (4.84-4.67)	70.61-3.64 (3.77-3.64)	28.42-3.20 (3.31-3.20)
R_{merge} (%)	8.3 (107.5)	7.6 (182.8)	5.2 (98.5)	7.4 (46.1)	6.2 (104.8)
$<I>/<\sigma(I)>$	10.6 (1.7)	13.5 (1.5)	15.2 (1.9)	16.1 (2.9)	11.1 (1.5)
Completeness (%)	99.9 (100.0)	99.8 (98.9)	98.2 (99.0)	84.5 (85.7)	98.9 (98.8)
Redundancy	6.7(6.7)	13.0 (13.3)	6.7 (7.2)	5.3 (4.8)	6.1 (6.2)
Refinement					
Resolution (Å)[a]	48.63-8.50 (8.81-8.50)	46.03 - 5.026 (5.20-5.02)	45.79-4.67 (4.84-4.67)	70.61-3.64 (3.77-3.64)	28.42-3.20 (3.31-3.20)
Number of reflections	1,672 (238)	3,756 (572)	4,428 (616)	24,059 (2,401)	24,325 (2,369)
R_{work}/R_{free} (%)	26.7 (47.6) /37.3 (41.9)	27.9 (39.5) /32.2 (39.2)	26.4 (38.0) /33.1 (40.9)	21.7 (28.3) /26.9 (31.4)	19.6 (33.6) /25.2 (38.2)
Number of atoms	8,508	4,313	4,349	17,284	8,742
RNA	7,460	3,789	3,789	15,149	7,586
Protein	1,048	524	524	2,096	1,048
Ion	0	0	36	29	86
Water	0	0	0	0	22
Mean *B* factor (Å^2)	480.4	246.9	243.8	117.2	128.0
RNA	482.1	253.8	238.3	109.6	118.7
Protein	468.2	196.7	274.2	172.9	192.7
Ligand/ion	n/a	n/a	373.5	66.8	176.4
Water	n/a	n/a	n/a	n/a	64.2
Rmsd					
Bond length (Å)	0.004	0.007	0.009	0.002	0.001
Bond angle (°)	0.82	1.27	1.68	0.49	0.37

[a]Highest resolution shell in parenthesis.

RNA 3′ termini, we observe Sr^{2+} frequently making bidentate inner-sphere interactions with the Hoogsteen faces of purines, making interactions at bulges and junctions where phosphates cluster, or bridging across the narrow major groove (Figure S1 available online). The presence of Sr^{2+} also aided the crystallization of the RNA component of the ribonuclease (RNase) P ribozyme (Torres-Larios et al., 2005), among others. Taken together, the ability of Sr^{2+} to bind RNA 3′ termini and its flexible coordination geometry are properties that may allow it to improve crystalline packing of RNA.

Sr^{2+} can also facilitate the identification of cation binding sites. Although anomalous scatterers such as metal hexammines or Ba^{2+} have been successfully soaked into RNA crystals for structure determination (e.g., Klein and Ferré-D'Amaré, 2006; Krasilnikov et al., 2004; Reiter et al., 2010; Ren et al., 2012; Serganov et al., 2004; Tereshko et al., 2003), the binding of these bulky complex ions can degrade RNA crystals. To further test the general utility of Sr^{2+} in RNA crystallography, we crystallized the adenine riboswitch (Serganov et al., 2004) in the presence of 150 mM Mg^{2+} and 50 mM Sr^{2+} (Experimental Procedures and Table 3). Bound Sr^{2+} ions were clearly visible in anomalous difference and residual Fourier syntheses, even with data collected at the selenium K edge (Figure 5). Compared to Mg^{2+}, which scatters X-rays weakly (comparable to water), the electron-rich Sr^{2+} can be readily observed even at low resolution. Data from a Sr^{2+}-soaked T-box cocrystal diffracting to only 4.7 Å reveals approximately the same number of well-defined bound Sr^{2+} ions as does a 3.2 Å data set, with most Sr^{2+} peaks above 4–6 SD in $|F_o|$-$|F_c|$ residual-electron-density maps.

Sr^{2+} also produces a robust anomalous signal and thus could facilitate the experimental phasing of RNA-only crystals. RNA crystallography lacks a universal de novo phasing strategy comparable to the ubiquitously used selenomethionine substitution (Hendrickson et al., 1990; Yang et al., 1990) developed for proteins. To date, phase information for RNA-only crystal structures are generally obtained by cocrystallization or postcrystallization soaking with a panel of electron-rich or anomalously scattering compounds, such as iridium (III) hexamine, cobalt (III) hexamine, or Ba^{2+}, at various concentrations. Although this trial-and-error approach does work for many RNAs, it is laborious and time consuming, and does not guarantee success. In situations such as crystals grown in the presence of high-ionic-strength or ammonium ions, soaking these heavy atoms rarely produces adequate occupancy to permit phasing (Keel et al., 2007). Directed soaking strategies, such as the use of engineered G•U motif to recruit hexammine ions, have helped phase several

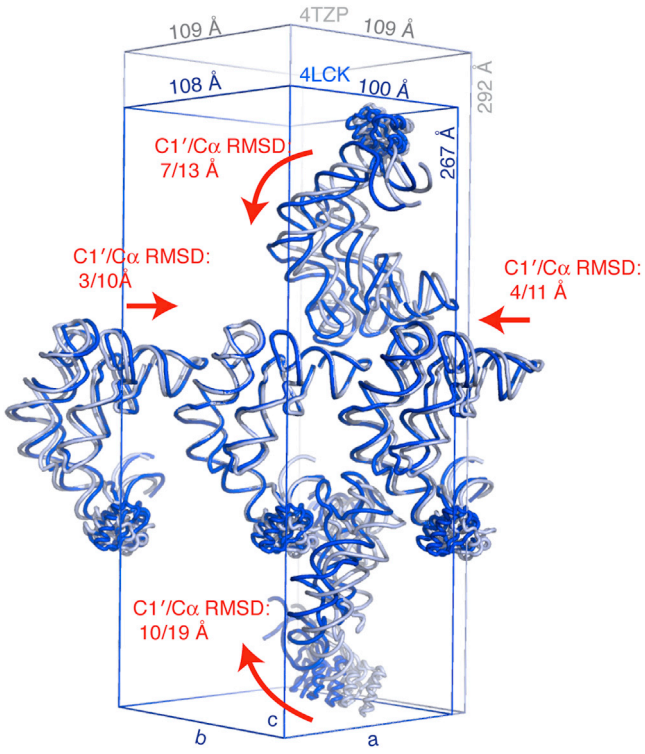

Figure 2. In-Crystal Redistribution of T-Box Ternary Complexes as Rigid Bodies Driven by Dehydration and Cation Replacement

Overlay of T-box ternary complexes in untreated (as-grown) crystals (light blue, Figure 1B, PDB code 4TZP) and fully dehydrated and cation-exchanged crystals (blue, Figure 1D, PDB code 4LCK). The corresponding crystallographic unit cells are also shown, indicating ~10% compression along both the *a* and *c* axes. The reference complexes in the center of the panel superimpose well (rmsd = 172, C1′ < 1.4 Å), but the neighboring four complexes shift substantially closer as a result of the postcrystallization treatment (rmsd ranges from 3 to 10 Å for RNA C1′ and from 10 to 19 Å for protein Cα). Red arrows denote directions of displacement (translation and rotation) of the four neighboring complexes.

novel RNA structures (Keel et al., 2007). The robust Sr^{2+} anomalous signal at both its K edge (16.1 keV, f′ 3.7 e) and CuKα (8.0 keV, f′ 1.8 e) wavelengths exceeds the routinely exploited protein-sulfur anomalous signal at the CuKα edge (f″ 0.56 e). This and the observation that moderately sized, soft Sr^{2+} prevalently binds RNA nucleobase, backbone phosphates, and 3′ termini without deforming the structure suggest that SAD phasing using Sr^{2+} may hold promise as a general, straightforward RNA phasing strategy that complements existing methods.

DISCUSSION

Several studies have reported on the utility of controlled dehydration for improvement of the diffraction properties of protein crystals and have investigated how protein molecules reorganized to form improved packing contacts (Deng et al., 2012; Heras and Martin, 2005; Russo Krauss et al., 2012). Using a similar approach, we have previously found that brief soaking in a high-osmolarity solution of crystals of the *glmS* ribozyme-riboswitch improved their diffraction limit (Klein and Ferré-D'Amaré, 2009; Klein et al., 2007) from 3.0 to 1.7 Å. Because proteins and nucleic acids are both extensively solvated, dehydration has the potential to improve the crystalline order of both. The cation-exchange strategy that we introduce here exploits the fact that, unlike most proteins, nucleic acids are surrounded and stabilized by a cationic counterion cloud, as well as site-specific-bound cations (Draper, 2004). Our findings with the T-box ternary complex suggests that the combination of cation exchange, Sr^{2+} soaking, and controlled dehydration (possibly assisted by mechanical support from agarose fibers in solvent channels) can be a powerful postcrystallization strategy to improve the crystalline order of large RNAs and also to facilitate the de novo phase determination and location of cation-binding sites.

It is noteworthy that in both cases of the *glmS* ribozyme and T-box-tRNA complexes in which RNA crystals responded favorably to dehydration treatments, PEG 3350 is a precipitant and dehydrating agent. In fact, PEGs of various molecular masses are the most commonly used dehydration agents among reports of successful protein-crystal dehydration (Russo Krauss et al., 2012). Nonetheless, a number of protein crystals have been successfully improved by dehydrating with non-PEG agents such as 3.5 M $(NH_4)_2SO_4$, 4.5 M NaCl, 2.0 M KCl, and saturated K_2CrO_4 (Heras and Martin, 2005; Russo Krauss et al., 2012). It remains unknown whether these salts can also act as dehydration agents to improve crystals containing predominantly RNA. Another consideration in applying this method with other RNAs is the observation that some RNAs may possess specific, structural, or functional Mg^{2+}-binding sites that may not accommodate the more bulky Sr^{2+}. Postcrystallization-treatment solutions containing various ratios of Mg^{2+} and Sr^{2+} may be attempted in these situations. In the case of the adenine riboswitch crystals grown in the presence of both Mg^{2+} and Sr^{2+}, Sr^{2+} did not replace Mg^{2+} in any of the five specific Mg^{2+}-binding sites but, instead, bound to a new site proximal to one of the Mg^{2+} sites (Figure 5). Due to the highly restricted octahedral coordination geometry of Mg^{2+}, many divalent cations cannot stably substitute for Mg^{2+} at specific Mg^{2+} sites.

Despite the empirical successes of postcrystallization treatments such as annealing and dehydration to improve the order of crystals of many proteins (Deng et al., 2012; Russo Krauss et al., 2012) and now RNAs, the structures of the pretreatment crystals have rarely been reported. Therefore, it has largely remained obscure how osmolarity changes trigger in-crystal movements or conformational changes of macromolecules. The precise nature of these molecular transitions and how the newly created crystal contacts are energetically or structurally superior to what was present in untreated crystals frequently remain undefined. In this study, the structural determination of a series of untreated, partially treated, and fully optimized RNA crystals allowed us to track macromolecular movements within crystals when the osmolarity is drastically changed. Our structures suggest that the formation of intimate stacking interactions and a stable A minor interaction were the key enablers of a drastically improved crystalline order for our T-box ternary-complex crystals. This finding is consistent with the central role of nucleobase stacking in stabilizing both RNA architecture and crystal contacts (Hermann and Patel, 1999; Zhang and Ferré-D'Amaré, 2014a; Zhang et al., 2010).

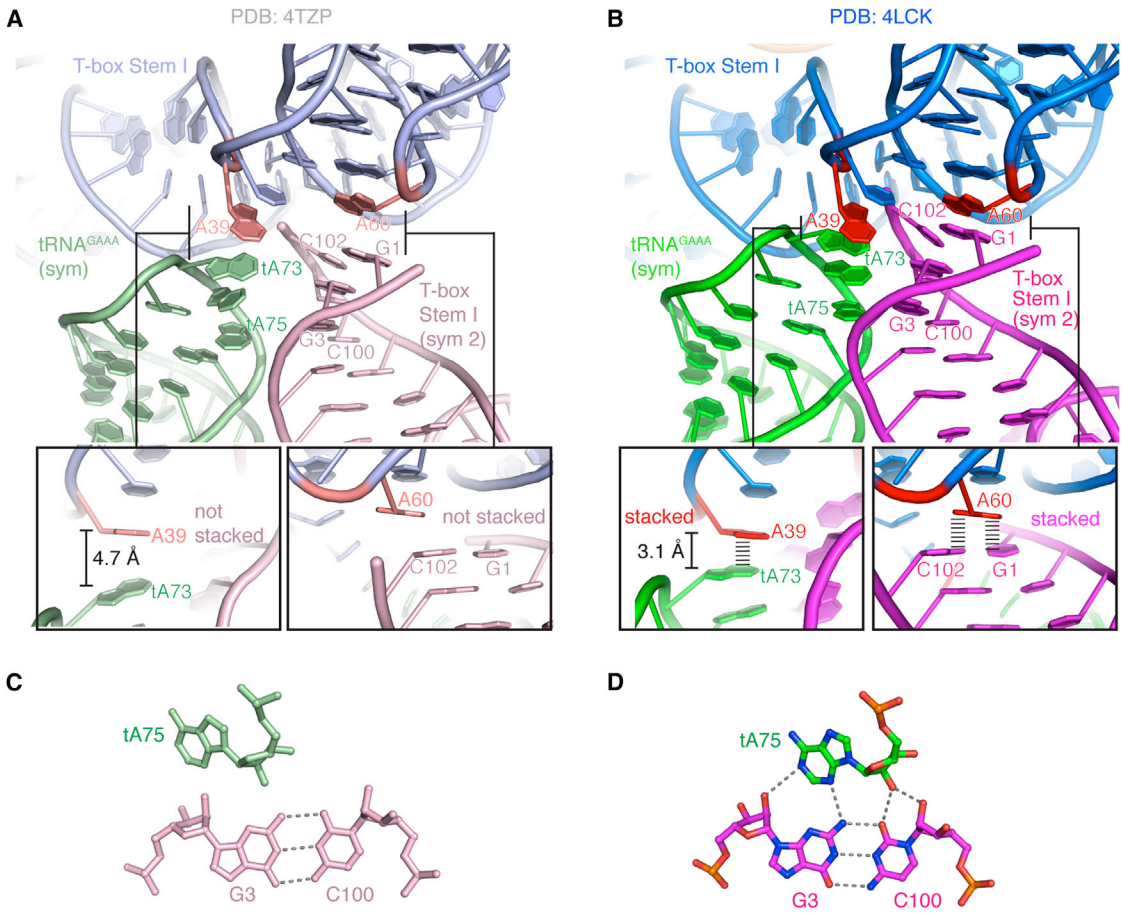

Figure 3. In-Crystal Movements of T-Box Ternary Complexes Produce Superior Crystal Contacts

(A) Detail of a major crystal contact in untreated crystals involving three symmetry-related ternary complexes, shown in light blue, pale green, and salmon, respectively. The rear face of the interdigited T-loops of Stem I distal region (opposite the face interacting with the tRNA elbow; Zhang and Ferré-D'Amaré, 2013) form a prominent flat surface available for crystal packing. Two patches of this flat surface, A39 and A60 (in deep salmon), are adjacent to but not in direct contact with the apical adenine of the GAAA tetraloop capping the tRNA acceptor stem (tA73, lower left inset) of a second complex (pale green), and with the terminal base pair of T-box Stem I (G1•C102, lower right inset) of a third complex (salmon), respectively.

(B) Detail of an improved crystal contact found in the same region in optimally treated crystals through cation replacement and dehydration. The figure is colored as in (A) but with more solid colors. Two neighboring complexes pack closer with the reference complex (top, marine) through translation and rotation (Figure 2), bringing tA73 into direct stacking distance (~3.1 Å) with A39, and the Stem I terminal G1•C102 into a direct stacking configuration with A60. Stacking interactions are indicated by parallel lines.

(C and D) The absence (C) and presence (D) of a class-I A-minor interaction between tA75 of the tetraloop of a tRNA and the minor groove of the proximal region of Stem I (G3•C100) in untreated and optimally treated crystals, respectively, colored as in (A) and (B). The tRNA residue numbers are preceded by "t." Gray dotted lines indicate hydrogen bonds.

In-crystal movements of macromolecules induced by dehydration and ion exchange are subject to the constraints of crystal packing and controlled by kinetic and thermodynamic parameters associated with increased desolvation; the disruption of existing packing contacts; and the formation of new, energetically more favorable packing interactions. Our comparative analyses show that, upon dehydration, T-box ternary complexes, such as the *glmS* ribozyme-riboswitch, primarily shift as rigid bodies by up to 19 Å (Klein and Ferré-D'Amaré, 2009). In the case of proteins, e.g., the heparan sulfate proteoglycan Glypican-1, dehydration drives rigid-body translation of the proteins by ~11 Å closer to the neighboring molecules, orders a previously disordered protease domain, and creates a new intermolecular interface of as much as 375 $Å^2$ (Awad et al., 2013). The observation that both protein and RNA molecules tend to redistribute as rigid bodies upon dehydration makes thermodynamic and structural sense because the large-scale conformational changes not only would have higher activation barriers that may not be overcome by the gain from additional favorable enthalpy from more intimate packing but may lead to a packing arrangement incompatible with the existing crystal lattice, thus causing mechanical stress to the crystals.

EXPERIMENTAL PROCEDURES

Cocrystallization of the T-Box Stem I-tRNA^{Gly}-YbxF Ternary Complex

Cocrystals were prepared as described (Zhang and Ferré-D'Amaré, 2013). Briefly, *O. iheyensis* tRNA^{Gly} (75 nucleotides, engineered by circular permutation

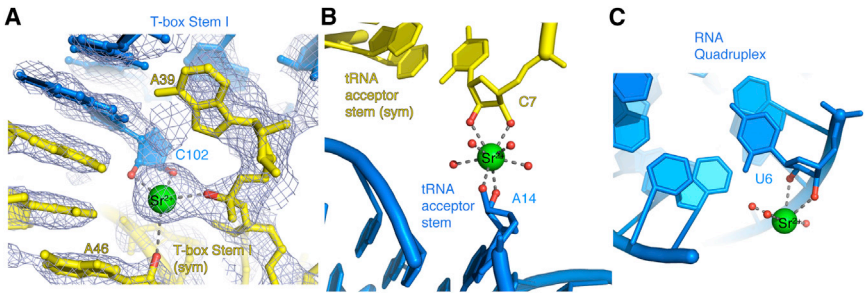

Figure 4. Interfacial Sr^{2+} Ions Bridge Symmetry-Related RNA Molecules by Binding to Their 3′ Termini

(A) A well-defined Sr^{2+} ion (green sphere) is shown bound to the *cis*-diol of the T-box RNA 3′ –terminal nucleotide (C102, marine) and to two nonbridging oxygen atoms of a symmetry-related T-box molecule (yellow) through inner-sphere coordination.

(B) Similar inner-sphere coordination between Sr^{2+} and two 3′ *cis*-diol groups in bridging two symmetry-related heptanucleotides derived from $tRNA^{Ala}$ acceptor stem. The nonbonded red spheres denote water molecules coordinated by Sr^{2+}.

(C) A Sr^{2+} is shown engaging in similar inner-sphere coordination with a 3′ *cis*-diol of a quadruplex-forming RNA.

See also Figure S1.

[Xiao et al., 2008] and the introduction of a terminal GAAA tetraloop [Zhang and Ferré-D'Amaré, 2014b]) was heated to 90°C in water for 3 min and cooled to 4°C over 2 min, mixed with one equivalent of *O. iheyensis glyQ* Stem I RNA and incubated in the presence of 50 mM HEPES-KOH (pH 7.0), 100 mM KCl, 20 mM $MgCl_2$, and 5 mM *tris*(2-carboxyethyl)phosphine (TCEP) at 50°C for 10 min and then at 37°C for 30 min. One equivalent of selenomethionyl *B. subtilis* YbxF (Baird et al., 2012) was then added. The solution was adjusted to 200 μM complex, 2 mM spermine, 0.2% (w/v) low-melting-point agarose and held at 37°C. For crystallization at 21°C by vapor diffusion, this complex solution was mixed 1:1 with a reservoir solution of 50 mM Bis-Tris (HCl) (pH 6.5), 300 mM Li_2SO_4, and 20% PEG 3350. Plate-shaped crystals grew in 1–4 weeks to maximum dimensions of 300 × 300 × 50 μm^3.

Table 3. Crystallographic Statistics of Adenine Riboswitch Structures

	PDB Accession Code	
	4TZX	4TZY
Data Collection		
Space group	$P2_12_12$	$P2_12_12$
Cell length: *a*, *b*, *c* (Å)	49.6, 152.8, 25.0	49.3, 152.3, 25.0
Cell angles: α, β, γ (°)	90, 90, 90	90, 90, 90
Resolution (Å)[a]	47.21-2.01 (2.13-2.01)	41.4-2.57 (2.72-2.57)
R_{merge} (%)	6.5 (97.1)	7.7 (64.1)
$\langle I \rangle / \langle \sigma(I) \rangle$	21.1 (2.1)	15.3 (2.0)
Completeness (%)	99.6 (99.3)	99.8 (99.7)
Redundancy	5.7 (5.2)	3.8 (3.8)
Refinement		
Resolution (Å)[a]	47.21-2.01 (2.08-2.01)	41.4-2.57 (2.66-2.57)
Number of. reflections	13466 (1341)	6534 (625)
R_{work}/R_{free} (%)	22.4 (35.9) /25.7 (37.5)	20.4 (35.6) /25.1 (38.5)
Number of atoms	1,632	1,542
RNA	1,502	1,502
Protein	0	0
Ligand/ion	19	19
Water	111	21
Mean *B* factor (Å^2)	45.8	52.6
RNA	46.1	52.6
Protein	n/a	n/a
Ligand/ion	37.7	65.3
Water	42.1	37.9
Rmsd		
Bond length (Å)	0.001	0.001
Bond angle (°)	0.35	0.32

[a]Highest resolution shell in parenthesis.

Preparation of Cocrystals of Adenine Riboswitch and Adenine

Cocrystals were prepared essentially as described (Serganov et al., 2004). Briefly, a 71 nt variant of the *add* adenine riboswitch RNA was produced using in vitro transcription and purified by denaturing urea-PAGE. For crystallization by vapor diffusion, a solution containing 700 μM RNA, 50 mM KOAc (pH 6.8), 2 mM $MgCl_2$, and 5 mM adenine was mixed 1:1 (v/v) with a reservoir solution of 2.8–3.0 M 1,6-hexanediol, 100 mM Tris HCl (pH 8.5), and either 200 mM $MgCl_2$ (PDB code 4TZX), or 150 mM $MgCl_2$ and 50 mM $SrCl_2$ (PDB code 4TZY). Crystals grew to maximal dimensions of 250 × 50 × 50 μm^3 in 5 days at 4°C and were directly flash-frozen by being plunged into liquid nitrogen.

Postcrystallization Treatments and Data Collection

Crystals of the T box ternary complex were transferred into glass depression plates filled with 150 μl of various postcrystallization treatment solutions (Table 1) and incubated for 16 hr at 21°C. Crystals were then dissected from the agarose using MicroSaws (Mitegen), mounted on 90°-bent MicroLoops (Mitegen), and vitrified by being plunged into liquid nitrogen. Crystallographic data were collected at 100 K at beamlines 5.0.1 and 5.0.2 of the Advanced Light Source (ALS), and at beamlines 24-ID-C and 24-ID-E of the Advanced Photon Source (APS) and reduced using X-ray Detector Software (XDS) (Kabsch, 2010) and SCALA (Evans, 2006) or HKL2000 (Otwinowski and Minor, 1997). The data-collection statistics are summarized in Table 2.

Structural Determination and Refinement

The structural determination of the T-box ternary complex at 3.2 Å using data from fully ion-replaced and dehydrated crystals has been described (Zhang and Ferré-D'Amaré, 2013). Structures of untreated and partially treated crystals were solved using molecular replacement with PHASER (McCoy et al., 2007) using the 3.2 Å structure (PDB code 4LCK) as the search model. Unambiguous solutions were obtained for each of the data sets, with overall translation function *Z* scores of 12.4, 16.7, 22.4, and 17.2 for the structures with PDB codes 4TZP, 4TZV, 4TZW, and 4TZZ, respectively. Structures of the *add*-riboswitch-adenine complex (non-Sr^{2+}, PDB code 4TZX; Sr^{2+}-containing, PDB code 4TZY) were solved using molecular replacement with PHASER using the published structure (Serganov et al., 2004; PDB code 1Y26) as the search model. Initial solutions were subjected to manual rebuilding (Emsley et al., 2010) interspersed with iterative rounds of rigid-body, simulated-annealing, and individual isotropic *B* factor refinement using PHENIX (Afonine et al., 2012). Because of limited resolution of the data, structure 4TZP was subjected only to rigid-body and translation-libration-screw (TLS) *B* factor refinement. The refinement statistics are summarized in Tables 2 and 3.

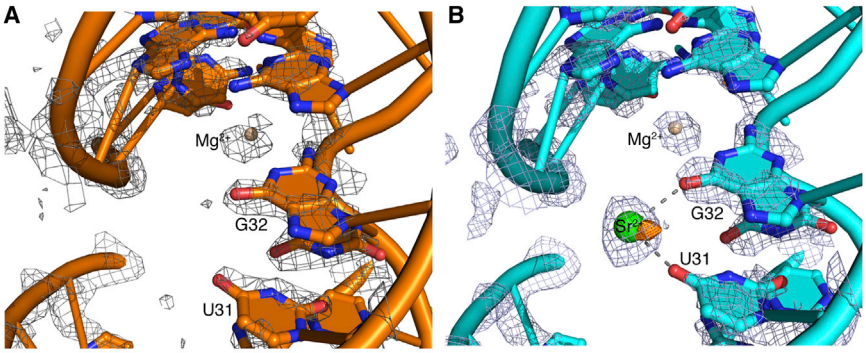

PDB: 4TZX PDB: 4TZY

Figure 5. A Representative Sr^{2+} Binding Site on the Adenine Riboswitch RNA

(A) A Mg^{2+} binding site on the *add* riboswitch RNA, gray mesh is a portion of the composite simulated-annealing-omit $2|F_o|-|F_c|$ electron-density map (2.0 SD).

(B) In addition to the bound Mg^{2+} in the same position as in (A), a new Sr^{2+} binding site appears in both in the composite simulated-annealing-omit $2|F_o|-|F_c|$ electron-density map (gray mesh, contoured at 2.0 SD) and the anomalous-difference Fourier map (orange mesh, contoured at 3.0 SD).

ACCESSION NUMBERS

Atomic coordinates and structure factor amplitudes have been deposited with the Protein Data Bank with accession codes 4TZP, 4TZV, 4TZW, 4TZZ, 4TZX, and 4TZY.

SUPPLEMENTAL INFORMATION

Supplemental Information includes one figure and can be found with this article online at http://dx.doi.org/10.1016/j.str.2014.07.011.

AUTHOR CONTRIBUTIONS

J.Z. and A.R.F. conceived and designed the experiments. J.Z. carried out all crystallization, postcrystallization treatments, diffraction-data collection, and refinement. Both authors analyzed data and wrote the manuscript.

ACKNOWLEDGMENTS

We thank the staff at beamlines 5.0.1 and 5.0.2 of the ALS and ID-24-C and ID-24-E of APS, in particular K. Perry and K. R. Rajashankar of the Northeastern Collaborative Access Team (NE-CAT) of the APS for support in data collection and processing; Y. Liu and Y.-X. Wang of the National Cancer Institute for providing the *add* riboswitch RNA; G. Piszczek, R. Levine, and D.-Y. Lee of the National Heart, Lung and Blood Institute (NHLBI) for assistance with biophysical and mass spectrometric characterization; and N. Baird, T. Hamma, C. Jones, M. Lau, A. Roll-Mecak, and K. Warner for discussions. This work is partly based on research conducted at the ALS on the Berkeley Center for Structural Biology Beamlines and at the APS on the NE-CAT Beamlines (supported by National Institute of General Medical Sciences grant P41GM103403). Use of ALS and APS was supported by the U.S. Department of Energy. This work was supported in part by the intramural program of the NHLBI, NIH.

Received: May 29, 2014
Revised: July 11, 2014
Accepted: July 28, 2014
Published: August 28, 2014

REFERENCES

Afonine, P.V., Grosse-Kunstleve, R.W., Echols, N., Headd, J.J., Moriarty, N.W., Mustyakimov, M., Terwilliger, T.C., Urzhumtsev, A., Zwart, P.H., and Adams, P.D. (2012). Towards automated crystallographic structure refinement with phenix.refine. Acta Crystallogr. D Biol. Crystallogr. *68*, 352–367.

Awad, W., Svensson Birkedal, G., Thunnissen, M.M., Mani, K., and Logan, D.T. (2013). Improvements in the order, isotropy and electron density of glypican-1 crystals by controlled dehydration. Acta Crystallogr. D Biol. Crystallogr. *69*, 2524–2533.

Baird, N.J., Zhang, J., Hamma, T., and Ferré-D'Amaré, A.R. (2012). YbxF and YlxQ are bacterial homologs of L7Ae and bind K-turns but not K-loops. RNA *18*, 759–770.

Chayen, N.E. (2004). Turning protein crystallisation from an art into a science. Curr. Opin. Struct. Biol. *14*, 577–583.

Chetnani, B., and Mondragón, A. (2013). Structural biology: RNA exerts self-control. Nature *500*, 279–280.

Deng, X., Davidson, W.S., and Thompson, T.B. (2012). Improving the diffraction of apoA-IV crystals through extreme dehydration. Acta Crystallogr. Sect. F Struct. Biol. Cryst. Commun. *68*, 105–110.

Draper, D.E. (2004). A guide to ions and RNA structure. RNA *10*, 335–343.

Emsley, P., Lohkamp, B., Scott, W.G., and Cowtan, K. (2010). Features and development of Coot. Acta Crystallogr. D Biol. Crystallogr. *66*, 486–501.

Evans, P. (2006). Scaling and assessment of data quality. Acta Crystallogr. D Biol. Crystallogr. *62*, 72–82.

Ferré-D'Amaré, A.R. (2010). Use of the spliceosomal protein U1A to facilitate crystallization and structure determination of complex RNAs. Methods *52*, 159–167.

Ferré-D'Amaré, A.R., and Scott, W.G. (2010). Small self-cleaving ribozymes. Cold Spring Harb. Perspect. Biol. *2*, a003574.

Ferré-D'Amaré, A.R., and Winkler, W.C. (2011). The roles of metal ions in regulation by riboswitches. Met. Ions Life Sci. *9*, 141–173.

Ferré-D'Amaré, A.R., Zhou, K., and Doudna, J.A. (1998). A general module for RNA crystallization. J. Mol. Biol. *279*, 621–631.

Grigg, J.C., Chen, Y., Grundy, F.J., Henkin, T.M., Pollack, L., and Ke, A. (2013). T box RNA decodes both the information content and geometry of tRNA to affect gene expression. Proc. Natl. Acad. Sci. USA *110*, 7240–7245.

Hendrickson, W.A., Horton, J.R., and LeMaster, D.M. (1990). Selenomethionyl proteins produced for analysis by multiwavelength anomalous diffraction (MAD): a vehicle for direct determination of three-dimensional structure. EMBO J. *9*, 1665–1672.

Heras, B., and Martin, J.L. (2005). Post-crystallization treatments for improving diffraction quality of protein crystals. Acta Crystallogr. D Biol. Crystallogr. *61*, 1173–1180.

Hermann, T., and Patel, D.J. (1999). Stitching together RNA tertiary architectures. J. Mol. Biol. *294*, 829–849.

Hofer, T.S., Randolf, B.R., and Rode, B.M. (2006). Sr(II) in water: A labile hydrate with a highly mobile structure. J. Phys. Chem. B *110*, 20409–20417.

Kabsch, W. (2010). XDS. Acta Crystallogr. D Biol. Crystallogr. *66*, 125–132.

Kazantsev, A.V., Krivenko, A.A., and Pace, N.R. (2009). Mapping metal-binding sites in the catalytic domain of bacterial RNase P RNA. RNA *15*, 266–276.

Keel, A.Y., Rambo, R.P., Batey, R.T., and Kieft, J.S. (2007). A general strategy to solve the phase problem in RNA crystallography. Structure *15*, 761–772.

Klein, D.J., and Ferré-D'Amaré, A.R. (2006). Structural basis of *glmS* ribozyme activation by glucosamine-6-phosphate. Science *313*, 1752–1756.

Klein, D.J., and Ferré-D'Amaré, A.R. (2009). Crystallization of the *glmS* ribozyme-riboswitch. Methods Mol. Biol. *540*, 129–139.

Klein, D.J., Wilkinson, S.R., Been, M.D., and Ferré-D'Amaré, A.R. (2007). Requirement of helix P2.2 and nucleotide G1 for positioning the cleavage site and cofactor of the *glmS* ribozyme. J. Mol. Biol. *373*, 178–189.

Krasilnikov, A.S., Xiao, Y., Pan, T., and Mondragón, A. (2004). Basis for structural diversity in homologous RNAs. Science *306*, 104–107.

Lorber, B., Sauter, C., Théobald-Dietrich, A., Moreno, A., Schellenberger, P., Robert, M.C., Capelle, B., Sanglier, S., Potier, N., and Giegé, R. (2009). Crystal growth of proteins, nucleic acids, and viruses in gels. Prog. Biophys. Mol. Biol. *101*, 13–25.

Matthews, B.W. (1968). Solvent content of protein crystals. J. Mol. Biol. *33*, 491–497.

McCoy, A.J., Grosse-Kunstleve, R.W., Adams, P.D., Winn, M.D., Storoni, L.C., and Read, R.J. (2007). Phaser crystallographic software. J. Appl. Cryst. *40*, 658–674.

Mueller, U., Schübel, H., Sprinzl, M., and Heinemann, U. (1999). Crystal structure of acceptor stem of tRNA(Ala) from *Escherichia coli* shows unique G.U wobble base pair at 1.16 A resolution. RNA *5*, 670–677.

Nissen, P., Ippolito, J.A., Ban, N., Moore, P.B., and Steitz, T.A. (2001). RNA tertiary interactions in the large ribosomal subunit: the A-minor motif. Proc. Natl. Acad. Sci. USA *98*, 4899–4903.

Otwinowski, Z., and Minor, W. (1997). Processing of X-ray diffraction data collected in oscillation mode. Methods Enzymol. *276*, 307–326.

Pan, B., Shi, K., and Sundaralingam, M. (2006). Crystal structure of an RNA quadruplex containing inosine tetrad: implications for the roles of NH2 group in purine tetrads. J. Mol. Biol. *363*, 451–459.

Reiter, N.J., Osterman, A., Torres-Larios, A., Swinger, K.K., Pan, T., and Mondragón, A. (2010). Structure of a bacterial ribonuclease P holoenzyme in complex with tRNA. Nature *468*, 784–789.

Ren, A., Rajashankar, K.R., and Patel, D.J. (2012). Fluoride ion encapsulation by Mg^{2+} ions and phosphates in a fluoride riboswitch. Nature *486*, 85–89.

Russo Krauss, I., Sica, F., Mattia, C.A., and Merlino, A. (2012). Increasing the X-ray Diffraction Power of Protein Crystals by Dehydration: The Case of Bovine Serum Albumin and a Survey of Literature Data. Int. J. Mol. Sci. *13*, 3782–3800.

Serganov, A., Yuan, Y.R., Pikovskaya, O., Polonskaia, A., Malinina, L., Phan, A.T., Hobartner, C., Micura, R., Breaker, R.R., and Patel, D.J. (2004). Structural basis for discriminative regulation of gene expression by adenine- and guanine-sensing mRNAs. Chem. Biol. *11*, 1729–1741.

Tereshko, V., Skripkin, E., and Patel, D.J. (2003). Encapsulating streptomycin within a small 40-mer RNA. Chem. Biol. *10*, 175–187.

Torres-Larios, A., Swinger, K.K., Krasilnikov, A.S., Pan, T., and Mondragón, A. (2005). Crystal structure of the RNA component of bacterial ribonuclease P. Nature *437*, 584–587.

Wan, Y., Kertesz, M., Spitale, R.C., Segal, E., and Chang, H.Y. (2011). Understanding the transcriptome through RNA structure. Nat. Rev. Genet. *12*, 641–655.

Xiao, H., Edwards, T.E., and Ferré-D'Amaré, A.R. (2008). Structural basis for specific, high-affinity tetracycline binding by an *in vitro* evolved aptamer and artificial riboswitch. Chem. Biol. *15*, 1125–1137.

Yang, W., Hendrickson, W.A., Crouch, R.J., and Satow, Y. (1990). Structure of ribonuclease H phased at 2 A resolution by MAD analysis of the selenomethionyl protein. Science *249*, 1398–1405.

Zhang, J., and Ferré-D'Amaré, A.R. (2013). Co-crystal structure of a T-box riboswitch stem I domain in complex with its cognate tRNA. Nature *500*, 363–366.

Zhang, J., and Ferré-D'Amaré, A.R. (2014a). Direct evaluation of tRNA aminoacylation status by the T-box riboswitch using tRNA-mRNA stacking and steric readout. Mol. Cell *55*, 148–155.

Zhang, J., and Ferré-D'Amaré, A.R. (2014b). New molecular engineering approaches for crystallographic studies of large RNAs. Curr. Opin. Struct. Biol. *26C*, 9–15.

Zhang, J., Lau, M.W., and Ferré-D'Amaré, A.R. (2010). Ribozymes and riboswitches: modulation of RNA function by small molecules. Biochemistry *49*, 9123–9131.